Integration of Scheimpflug-based Corneal Tomographic and Biomechanical Assessments for Enhancing Ectasia Detection

Renato Ambrósio Jr, MD, PhD[1,2,3]; Bernardo Lopes, MD[1,2]; Fernando Faria-Correia, MD[1,4]; Marcella Q. Salomão, MD[1,2]; Jens Bühren, MD[5]; Cynthia J. Roberts, PhD[6]; Ahmed Elsheikh, PhD[7]; Riccardo Vinciguerra, MD[8,9]; Paolo Vinciguerra, MD[10,11]

1. Rio de Janeiro Corneal Tomography and Biomechanics Study Group; Rio de Janeiro, Brazil
2. Department of Ophthalmology, Federal University of São Paulo; São Paulo, Brazil
3. Department of Ophthalmology, Pontific Catholic University of Rio de Janeiro; Rio de Janeiro, Brazil
4. School of Health Sciences, University of Minho, Braga, Portugal
5. Augenpraxisklinik Triangulum; Hanau, Germany
6. Department of Ophthalmology & Visual Science, and Department of Biomedical Engineering, The Ohio State University; Columbus, OH, USA
7. School of Engineering, University of Liverpool – Liverpool, United Kingdom
8. Department of Surgical Sciences, Division of Ophthalmology, University of Insubria; Varese, Italy
9. Department of Corneal and External Eye Diseases, St. Paul's Eye Unit, Royal Liverpool University Hospital, Liverpool, United Kingdom
10. Eye Center, Humanitas Clinical and Research Center, Via Manzoni 56, Rozzano (MI); Italy
11. Vincieye Clinic; Milan, Italy

Corresponding author: Renato Ambrósio Jr, MD, PhD dr.renatoAmbrósio@gmail.com; phone/fax +5521 2234-4233

Rua Conde de Bonfim 211/712 – Rio de Janerio, RJ – 20.520-050, Brazil

Financial Disclosure(s): Dr. Ambrósio, Dr. P. Vinciguerra, and Dr. Roberts are consultants for OCULUS Optikgeräte GmbH (Wetzlar, Germany). Dr. Bühren has received lecture fees from OCULUS; Dr. Elsheikh has received research funding from OCULUS Optikgeräte GmbH. “None of the remaining authors have any financial disclosures”

Running head: Tomographic/Biomechanical Index (TBI) for Ectasia detection

PRECIS

In a multicenter study, the TBI was developed using random forest method with leave-one-out cross-validation (RF/LOOCV) for combining parameters from Scheimpflug-based corneal tomography and biomechanical assessments for enhanced ectasia detection.

Acknowledgments

The authors thank Dr. Sven Reisdorf, PhD and Dr. Andreas Steinmuller, MSc (OCULUS) for the overall support in processing the data along with the helpful discussions and calculations. The Corvis ST instruments used in this study were provided by Oculus.

ABSTRACT

Purpose: To present the Tomographic/Biomechanical Index (TBI), that combines Scheimpflug-based corneal tomography and biomechanics for enhancing ectasia detection. **Methods:** Patients from different continents were studied. One eye randomly selected from 480 patients with normal corneas and from 204 keratoconus patients comprised groups I and II respectively. Group III included 72 non-operated ectatic eyes from 94 patients with very asymmetric ectasia, whose fellow eyes (group IV) presented with normal topography. Pentacam HR and Corvis ST (OCULUS; Wetzlar, Germany) parameters were analyzed and combined using different artificial intelligence methods (AI). The accuracies for detecting ectasia of BAD-D (Belin/Ambrósio Deviation) and CBI (Corvis Biomechanical Index) were compared to TBI, considering the areas under receiver operating characteristic curves (AUROC). **Results:** The random forest method with leave-one-out cross-validation (RF/LOOCV) provided the best AI model. The AUROC for detecting ectasia (groups II, III and IV) of TBI was 0.996, being statistically higher (DeLong, $p<0.001$) than BAD-D (0.956) and CBI (0.936). TBI cutoff value of 0.79 provided 100% sensitivity for detecting clinical ectasia (groups II and III) with 100% specificity. Considering group IV, AUROC for TBI, BAD-D and CBI were 0.985, 0.839 and 0.822 (DeLong, $p<0.001$). An optimized TBI cutoff value of 0.29 provided 90.4% sensitivity in group IV, with 96% specificity. **Conclusion:** TBI generated by RF/LOOCV provides accuracy for detecting ectasia, exceeding other techniques. TBI is sensitive for detecting sub-clinical (fruste) ectasia among eyes with normal topography in very asymmetric patients. TBI may also confirm unilateral disease, potentially epitomizing the inherent ectasia susceptibility of the cornea.

INTRODUCTION

The detection of mild or sub-clinical forms of ectatic corneal diseases (ECD) has gained momentous relevance because these cases are at very high risk for developing iatrogenic progressive ectasia (keratectasia) after corneal Laser Vision Correction (LVC) procedures.[1,2] Ectasia progression after LVC occurs due to the biomechanical decompensation of corneal stroma, which is related to two different factors: the preoperative predisposition or biomechanical status of the cornea, and the structural impact from the surgical procedure. The impact from the LVC procedure may be evaluated using different parameters including the residual stromal bed (RSB) and the percent of tissue altered (PTA).[3-6] In fact, the current concept is that when screening for ectasia risk among candidates for LVC, the surgeon should consider the inherent ectasia susceptibility of the cornea, which goes beyond (not over) the detection of mild cases with ECD.[2] Besides elective Refractive Surgery, augmenting sensitivity for identifying mild forms of ectasia at early clinical stage and monitoring disease progression have become of utmost importance because of the definitive paradigm shift in the management of ECD, which is related to the introduction of novel therapeutic approaches such as corneal crosslinking (CXL) techniques and intrastromal corneal ring segments (ICRS) implantation.[7,8]

The last three decades witnessed a factual revolution in corneal imaging, which includes the development of high resolution technologies capable of detailed characterizations of different aspects of corneal shape and anatomy, and the introduction of scientifically validated methods for representing and interpreting the generated data for improving the clinical decision process.[9] Placido-disk based corneal

topography characterizes the anterior or front corneal surface in detail, which enables the detection of abnormal patterns of corneal shape that accompany mild forms of keratoconus in cases in which routine examination shows no abnormal findings.[10] Such augmentation of sensitivity to detect ectasia among eyes with normal slit-lamp biomicroscopy and normal distance corrected visual acuity (DCVA) has positioned corneal topography as a mandatory exam for screening ectasia risk prior to LVC.[1,2,10] However, there are still cases that undergo ectasia progression after LVC procedures, even for low to mild corrections, despite relatively normal topography findings prior to LASIK,[11-13] surface ablation,[14] or SmILE (Small-Incision Lenticule Extraction).[15]

Front surface corneal analysis (topometric or topography) evolved into the three-dimension (3D) tomographic characterization, which typifies elevation of the front and back surfaces along with thickness mapping.[16] Eyes with normal topometric findings from patients with clinical ectasia detected in the fellow eye have been commonly studied to demonstrate the improved ability of corneal tomography to detect ECD.[17-19] In addition, the ability of tomographic data to augment the ability to detect ectasia risk or susceptibility in retrospective analysis of cases that developed keratectasia after LASIK.[12,20,21] Further advances on corneal imaging allowed for segmental or layered tomographic (3D) characterization with epithelial,[22,23] and Bowman's layer thickness mapping.[24]

Nevertheless, beyond shape analysis, clinical biomechanical assessment has been considered as an ultimate tool for enhancing the overall accuracy for identifying mild forms of ECD, along with the characterization of the inherent susceptibility of the cornea for ectasia progression.[12,21] In fact, there is a consensus that the

pathophysiology of corneal ectasia is related to altered biomechanical properties.[8] In addition, the current concept as proposed by Roberts and Dupps[25] is that a focal abnormality in corneal biomechanical properties precipitates a cycle of decompensation, leading to secondary localized thinning and steepening (bulging), which generates optical aberrations.[25] The Reichert Ocular Response Analyzer (ORA), a non-contact tonometer (NCT) that monitors corneal deformation through an infrared apical reflex, was introduced as the first clinical tool for *in vivo* biomechanical assessment.[26] Even though ORA first generation pressure-dependent parameters – corneal hysteresis (CH) and corneal resistance factor (CRF) provided relatively low sensitivity and specificity for discriminating keratoconic from normal corneas,[27] parameters derived from the corneal deformation signal were characterized, providing higher accuracy.[28] Interestingly, such data were found useful to improve diagnostic accuracy for mild forms of ECD when combined with tomography data.[21,29]

The Corvis ST (OCULUS Optikgeräte GmbH; Wetzlar, Germany) is also an NCT, but utilizes an ultra-high speed (UHS) Scheimpflug camera to monitor the deformation of the cornea in greater detail, with a collimated air pulse and fixed pressure profile.[30] While the first set of parameters derived from the Corvis ST measurement were found to have a relatively poor discriminant ability to detect ectatic diseases,[31-33] novel parameters such as the inverse concave radius of curvature during the concave phase of the deformation response, the deformation amplitude ratio between the apex and at 2mm from the apex (DA Ratio 2mm) and the stiffness parameter at first applanation (SPA1) were found to improve detection of ECD.[34,35] As described by Vinciguerra and coworkers,[36] the Corvis Biomechanical Index (CBI) was developed using linear

regression analysis (LRA) for combining parameters from the deformation corneal response (DCR) and from the horizontal thickness profile,[37] leading to high accuracy to detect clinical keratoconus.[36] Besides detection of ECD, the characterization of the deformation response has also provided an equation for intraocular pressure (IOP) correction, reducing reliance of IOP measurements on both corneal thickness and age.[38] The purpose of the current study was to develop a combined parameter based on Scheimpflug imaging to advance the ability to detect clinical and sub-clinical ectasia, using corneal tomography data from the Pentacam (OCULUS Optikgeräte GmbH; Wetzlar, Germany)[18] and biomechanical assessment from the Corvis ST.

Methods

Eight hundred and fifty eyes from 778 patients were included in this multicenter retrospective study. The patients were enrolled from two clinics located in two different continents: *Instituto de Olhos Renato Ambrósio* in Rio de Janeiro (Brazil), and the Vincieye Clinic in Milan (Italy). Institutional review board (IRB) from Humanitas Clinical and Research Center (Milan, Italy) ruled that approval was not required for the retrospective chart review study. The ethics committee of the Federal University of São Paulo approved this retrospective research study, which was conducted in accordance with the standards set in the 1964 Declaration of Helsinki, and revised in 2000. The eyes were divided into four groups. Group I (N) included one eye randomly selected from 480 patients with normal corneas. Group II (KC) was comprised of one eye randomly selected from 204 keratoconus patients. One eye was randomly included per patient in order to avoid selection bias related to the use of both eyes from the same subject.[39] Seventy-two non-operated eyes with clinical ectasia from 94 patients with very or highly asymmetric ectasia (VAE) were included in Group III (E-VAE), whose fellow eyes presented with normal topography (Group IV – NT-VAE). Twenty-two (22/94) very asymmetric ectasia cases had one or more surgical procedures such as CXL and ICRS implantation in the ectatic eye prior to the study, and were not included in Group III because these cases did not have a Corvis ST measurement preoperatively.

All patients had a comprehensive ophthalmic examination, including the Corvis ST and Pentacam HR (OCULUS Optikgeräte GmbH; Wetzlar, Germany) exams with

acceptable quality for proper analysis. Soft contact lens wear was discontinued for at least three days prior to the exam and rigid or hybrid contact lenses were discontinued for a minimal period of three weeks. The inclusion criteria for being a normal case (Group I) was to have normal corneas on the general eye exam in both eyes, including normal slit-lamp biomicroscopy, DCVA of 20/20 or better, overall subjective normal topography and tomography exams with no previous surgery and no use of topical medications different than artificial tears in both eyes. Keratoconic eyes included in this study were diagnosed with clinical ectasia in both eyes without any previous ocular procedures, such as CXL or ICRS implantation.[40,41] The criteria for clinical diagnosis of ectasia included topographic characteristics, such as skewed asymmetric bow-tie, inferior steepening and at least one slit lamp finding (Munson's sign, Vogt's striae, Fleischer's ring, apical thinning, Rizutti's sign).[41] Patients were considered as very asymmetric if the diagnosis of ectasia was confirmed in one eye based on the previously described criteria and the fellow had a normal front surface curvature (topometric) map. Objective criteria for considering normal topography was rigorously applied for defining the cases of Group IV, including KISA% lower than 60 and a paracentral inferior–superior (I-S value) asymmetry value at 6mm (3mm radii) less than 1.45.[42] These criteria avoid problems related to the subjectivity and inter and intra-examiner variability of the classifications of topographic maps.[43] All cases from each clinic had the tomographic data blindly re-evaluated by an expert on Anterior Segment from the other center (R. Ambrósio and P. Vinciguerra) for confirming inclusion criteria.

All measurements from the Corvis ST and Pentacam HR were taken by an experienced technician. Proper exam quality was assured by a manual, frame-by-frame

analysis of each exam, made by an independent masked examiner to ensure quality of each acquisition, including good edge detection over the whole deformation response or rotating Scheimpflug images, with the exclusion of severe alignment errors (x-direction), and blinking errors. Data from Pentacam HR and Corvis ST were exported to a custom spreadsheet using special research software.

Statistical Analysis

Statistical analyses were performed by different software packages: MedCalc Statistical Software version 16.8.4 (MedCalc, Ostend, Belgium https://www.medcalc.org), SPSS version 23 (IBM Corp. in Armonk, NY, USA), the R Core Team version 3.3.1.2016 (R Foundation for Statistical Computing, Vienna, Austria. URL https://www.R-project.org/), and a custom-written MATLAB program (R14, The MathWorks, Natick, MA, USA).

The data were analyzed and combined using different artificial intelligence methods (AI) including logistic regression analysis (LRA) with forward stepwise inclusion, support vector machine (SVM) and random forest (RF).[39,44] These methods were employed to optimize the ability to distinguish normal corneas (group I) from ectatic cases (groups II, III and IV) by the combination of parameters from corneal deformation response (CDR) and tomography, including Corvis Biomechanical Index (CBI),[36] and BAD-D (Belin/Ambrósio Deviation).[12,18,21,34,45-48] Considering the combined parameters were programed to have their output values as a continuous number

ranging from zero to one, an LRA function was created only using the BAD-D as the input parameter to calculate BAD-DI in order to facilitate comparisons. The leave-one-out cross-validation (LOOCV) technique was chosen for validation. In this method, a new model is built as many times as the number of cases included in the study. Each different model is built for all cases excluding one subject in which the model is tested. The results of the non-included cases in each of the 850 built models provide the output values of the LOOCV. Thereby, the validation model refers to the different models there were built with the leave-one-out strategy. Considering the number of false positive and false negative cases, the model would be validated or not. Once the model is properly validated for its generalized performance, a definitive algorithm would be built for all cases, which is expected to provide a more optimistic performance, but possibly with some degree of overfitting. However, it is expected that the results from the LOOCV provide a more realistic estimation of the performance when the model is applied in a novel population.

The Kolmogorov-Smirnov goodness-of-fit test and D'Agostino-Pearson test were applied for checking normal distributions. Spearman rank correlation test was used to measure the degree of association between age and TBI. ANOVA was used to test differences for age among the groups. Considering all indices in the keratoconus group were non-normally distributed, the analyzed parameters were compared among the groups using the non-parametric Kurskal-Wallis test, followed by the post hoc Dunn’s test to compare each pair of groups. The discriminative ability of each parameter was assessed by Receiver operating characteristic (ROC) curves. For each parameter tested, the area under the ROC curve (AUROC) was calculated and the best cutoff

value that yielded the highest accuracy is determined along with the sensitivity and specificity. Pairwise comparisons of the AUROC were accomplished with nonparametric approach as described by DeLong and coworkers for comparing the performance of diagnostic tests.[49] Furthermore, separation curves that display accuracy as a function of shifting the cut off value were plotted as described by Bühren.[50] This method allows for comparisons among the different metrics by using normalized cut points by a *Z* transformation with the optimum cutoff set to zero. The area under the separation curve (AUSEP) was calculated between the *x* limits of -2 and 2 standard deviations and *y* limits of 50 and 100% accuracy. Thus, higher AUSEP values indicate a high discriminative ability with a high tolerance to shifts of the critical cutoff value.[50] For ROC analysis a custom-written MATLAB program (R14, The MathWorks, Natick, Mass.) was used to confirm results obtained by MedCalc.

Results

A total of three hundred and sixty-four patients (227 healthy, 111 keratoconus and 26 cases with very asymmetric ectasia [VAE]) were enrolled from the Rio de Janeiro Corneal Tomography and Biomechanics Study Group at *Instituto de Olhos Renato Ambrósio* in Rio de Janeiro, Brazil. Four hundred and fourteen patients were enrolled from the Vincieye Clinic in Milan, Italy (253 healthy, 93 keratoconus and 68 cases with VAE). Table 1 summarizes the demographic characteristics of the groups. Females accounted for 57.5% of normal patients, while there were 64.43% of males among ectasia patients. There were no statistically significant differences for age among the groups (ANOVA, p=0.273). However, there was a broader range in the normal group.

Table 2 summarizes the descriptive statistics of the most important parameters among the groups. Central and minimal corneal thickness values, and maximal (KMax) keratometric values were normally distributed among normal eyes (p>0.5). Central (apex) thickness averaged 558µm with 30.1µm of standard deviation, ranging from 470 to 674 µm. Mean thinnest pachymetry was 552µm with 30µm of standard deviation, ranging from 467 to 646µm. The average difference between central and thinnest point values was 5.8µm with 4µm of standard deviation, ranging from 0 to 24µm, with 10.4% of cases having over 10µm difference and 3.1% having over 15µm difference. Mean maximal keratometry (Kmax) was 44.38D with 1.54D of standard deviation, ranging from 40.2 to 48.5D. Eighteen eyes (3.75%) in the normal group had a positive topometric keratoconus classification (TKC).[51] Six cases (1.25%) had an I-S value higher than 1.45 and 1 case (0.21%) had KISA% higher than 60. Mean BAD-D was

0.745 with 0.56 standard deviation, ranging from -1.13 to 2.35. Twenty eyes from group I (4.6%) had BAD-D values higher than 1.6 and 82 eyes (17.1%) had BAD-D values higher than 1.26 among normal eyes. CBI[36] was higher than 0.5 in 2.5% of normal cases (false positives).

All frank ectasia cases (groups II and III) had abnormalities detected by corneal topography that fulfilled criteria for diagnosis.[41,42] However, forty-eight cases (17.4%) had Kmax lower than 47.5D and 23 cases (8.7%) had Kmax lower than 46D. The Oculus topometric classification for keratoconus (TKC)[51] distribution was negative for 13 cases (4.7%). Eighty-nine cases (32.2%) were classified as grade 1, 78 (28.3%) as grade 2, 67 (24.3%) as grade 3 and 29 (10.5%) cases were classified as grade 4 ectasia. Four frank ectatic cases (1.4%) had BAD-D lower than 1.6, 14 cases (5.1%) had I-S value lower than 1.45D and 40 cases (14.5%) had KISA% lower than 60. CBI[36] was higher than 0.5 in 94.2% of frank ectatic eyes.

All eyes included in group IV were objectively determined to have normal topography (NT-VAE), having I-S value lower than 1.45D, KISA% lower than 60 and no positive TKC value.[42] Figure 1 displays the front surface axial or sagittal curvature (topometric) maps using Smolek-Klyce absolute 1.5D scale from the 94 NT-VAE cases. BAD-D was higher than 1.6 in 40 cases (42.6%) and higher than 1.26 in 64 cases (68.1%). Thirty-five (37.2%) cases in group IV had CBI higher than 0.5 and 42 cases (44.7%) had CBI higher than 0.3.

Three different artificial intelligence approaches were applied for combining data from corneal deformation response (Corvis ST) and corneal tomography (Pentacam)

298 data using leave-one-out cross-validation (LOOCV). Indices were determined from the
299 logistic regression analysis (LRAI) with forward stepwise inclusion, support vector
300 machine (SVMI) and random forest (RF). The most accurate method was the random
301 forest which is referred to as the TBI. A linear regression formula was applied for
302 normalizing BAD-D into an index, with outputs ranging from zero to one (BAD-DI). The
303 BAD-DI formula included a constant and a coefficient for BAD-D (y = a + b*x): 2.85958
304 (constant) + (-4.84877 * BAD-D), so that BAD-D and BAD-DI have a perfect correlation.
305 However, this approach facilitates comparison with other parameters as seen in Figure
306 2, which display the dot-plot graphs for the BAD-D, BAD-DI, CBI, and TBI.

307 Table 2 includes the mean, standard deviation, median and range (minimum –
308 maximum) for the main parameters, including BAD-D, BAD-DI, CBI, LRA, SVMI and
309 TBI. Results of Kruskal–Wallis one-way analysis of variance demonstrated differences
310 among the studied groups for all studied parameters ($p<0.000001$), which was
311 confirmed by Jonckheere-Terpstra trend test ($p<0.00001$). Post-hoc Dunn´s test results
312 were similar for all parameters, confirming differences among all paired groups
313 ($p<0.001$), with the exception of the comparison between keratoconus and ectatic eyes
314 from the very asymmetric cases (group II x group III [KC x VAE-E]).

315 Table 3 summarizes the results of receiver-operating characteristic (ROC) curve
316 analysis and the area under the separation curve (AUSEP) calculated between the
317 limits of -2 and +2 standard deviations. The analysis was performed for testing the
318 discriminating abilities to separate normal cases and all diseased cases (Table 3A),

normal cases from the cases with frank ectasia (table 3B) and normal cases with the supposed subclinical cases (table 3C). These data correlate to Figure 3 (A-C).

The TBI results presented refer to the outputs of the random forest method with leave-one-out cross-validation (RF/LOOCV) strategy, which provided the highest accuracy compared to LRA and SVM. The AUROC of the TBI for detecting ectasia (groups II, III and IV) was 0.996. The cut off value of 0.48 correctly classified 97.5% of the cases, having 98.8% specificity with 96.2% sensitivity. TBI had 100% sensitivity to detect frank ectasia cases (AUROC=1.0; groups II and III) with no false positives among the normal cases with optimal cut off values ranging from 0.75 to 0.81. Considering the ability to detect the eyes with normal topography from patients with clinical ectasia in the fellow eye, optimization of cut off value to 0.29 provided 90.4% sensitivity with 4% false positives (96% specificity; AUROC=0.985). TBI had a statistically higher AUROC (DeLong, $p<0.001$) than all other parameters for every analysis performed, except for the comparisons with BAD-D for detecting clinical ectasia cases (groups II and III), in which TBI had AUROC of 1.0 and BAD-D (and BAD-DI) had 0.997 (DeLong; $p=0.1198$). However, the AUSEP for BAD-D and BAD-DI were respectively 64 and 95, while TBI was 112. Such difference in AUSEP potentially confirms the higher discriminating ability of TBI than BAD-D to distinguish normal and clinical ectatic cases despite the non-significant differences found among the AUROC (Table 3). TBI had a significant negative correlation with age ($p<0,0001$; Spearman's coefficient of rank correlation [rho] = -0.18).

The ‘final’ random forest algorithm that is programmed and included in the commercial Oculus software is based on an optimized algorithm that included all 850 cases in the training set. This output provided an effectively perfect accuracy, reaching an AUROC of 1.0 for all subgroup comparisons in the current study. Considering the highest value for normal cases was 0.34 and the lowest values for frank ectatic cases (groups II and III) and for the cases in group IV were respectively 0.91 and 0.37, the cut off value of 0.35 correctly classified 100% of the cases. Interestingly, the correlation of the output of the TBI with LOOCV and the final model was highly significant ($p<0.0001$; Spearman's coefficient of rank correlation [rho] = 0.887).

Discussion

In this study, we introduce the TBI (Tomographic/Biomechanical Index) as a novel parameter based on a robust and innovative combination of data derived from Scheimpflug based corneal tomographic and biomechanical analysis. The TBI is derived from Pentacam HR and Corvis ST exams, resulting in higher accuracy for detecting ECD than all previous analyzed parameters. This was confirmed by analyzing the AUROC and AUSEP curves (Figures 2 and 3). While, it is important to include cases with mild or sub-clinical forms of ECD to facilitate appreciation of the clinical benefit for the novel parameter, the AUROC of TBI was statistically higher than all other analyzed parameters including CBI, when considering the detection of cases with clinical ectasia (groups II and III). As demonstrated by Vinciguerra and coworkers,[36] CBI was accurate for detecting clinical ectasia cases, with 16 false negative cases (5.7%) and 97.5% specificity, and AUROC of 0.977 which was statistically lower than TBI. In addition, the analysis of the separation curves (AUSEP) potentially reveals the benefits of TBI over metrics that are indeed highly accurate. For example, the BAD-D[12,18,21,34,45-48] had 98.2% sensitivity to detect clinical ectasia with less than 1% false positives (99.2% specificity) among normal eyes in the current study. The AUROC of BAD-D (and BAD-DI) was 0.997 which is not significantly lower than the one for TBI (AUROC=1.0) accordingly to DeLong's test to compare AUROC.[49] However, the analysis of the separation curves as described by Bühren[50] discloses a more dichotomous response characteristic of the TBI (Figure 2D), which is more tolerant to shifts on the cut off criterion compared to BAD-D and BAD-DI (Figure 2A).

The study included a large cohort of patients with normal corneas and with different levels of ectatic corneal disease (ECD). In order to avoid selection bias related to the use of both eyes from the same subject, we included one eye randomly selected per patient in groups I and II.[39] Seventy two patients had one eye in group III and the other eye in group IV. While these patients had both eyes included, these cases were by definition highly asymmetric, which avoids the problems related to enantiomorphism or similarities between right and left eyes. Considering the limitations of subjective interpretation of corneal topography maps,[43] we were restricted to applying front surface curvature indices as described by Rabinowitz[42] for objectively defining the inclusion criteria of group IV. Interestingly, even after twenty-three cases from the preliminary set of group IV were reclassified into group II due to the above criteria, some cases from group IV would still be found with suspicious curvature maps (Figure 1).

The current study included 94 eyes that reached objective criteria for normal corneal topography from patients with clinical ectasia in the fellow eye. This constitutes one of the largest cohort studies including such a special group of cases.[17-19,52] TBI was sensitive to detect abnormalities among 90.4% of cases in Group IV with less than 5% false positives. However, while these cases have been referred to as forme fruste keratoconus by Klyce,[53] it is important to consider that some of these cases may be true unilateral ectasia cases.[54] Remarkably, there is a consensus that true unilateral keratoconus does not exist, but also that secondary, induced ectasia caused by a pure mechanical process, such as eye rubbing, may occur unilaterally.[8] These ideas are in agreement with the two-hit hypothesis, which put forward the concept of ectasia to result from an underlying genetic predisposition along with external environmental

394 factors, including eye rubbing and atopy.[7] Our hypothesis is that TBI may reflect the
395 inherent susceptibility of the cornea to ectasia progression.

396 A possible study for assessing ectasia susceptibility involves the analysis of the
397 preoperative state of cases that developed ectasia after LVC along with the surgical
398 parameters which represent the impact from surgery on the cornea.[20] Another possible
399 approach is to integrate finite element simulations with the corneal structural and shape
400 analysis. In addition, adding longitudinal analysis for a retrospective evaluation of
401 patients that progressed to clinical ectasia would further improve criteria to define such
402 a group.[21] Even though we included a relatively large number of cases with mild ECD,
403 50% of the cases from groups II and III had Kmax lower than 52D and 65% had TKC
404 grade 2 or lower.

405 A limitation of the current cohort may be the criteria for inclusion in Group I. Even
406 though this is expected to be relatively rare, it is possible that some eyes with a normal
407 clinical exam, including corneal topography and tomography, have mild or susceptible
408 forms of ectasia such as in cases that progressed to keratectasia after different LVC
409 procedures.[11-15] The preoperative state of stable cases with long term follow up after
410 LVC would provide a more robust population for the normal control group.[17,20,34]

411 The random forest method provided the most efficient strategy for developing
412 TBI. In this advanced compound artificial intelligence based model, analysis starts like
413 an ordinary decision tree. This includes successive nodes defined by independent
414 variables with objective decisions based on cut off values. As in a classic decision tree,
415 the analyzed case is successively split into two mutual subgroups (branches) that

subdivide until a final decision of class assignment (leaves). The random forest takes this approach to the next level by combining numerous trees with the concept of an ensemble or cooperative effort. The algorithm grows the trees by sampling the data into random subgroups. Some input variables are also randomly selected to test their capability of splitting the data at each node. The predictor variable that provides the best split, according to an objective function is applied on each node. Each tree gets a "vote" in classifying. The final classification is based on the votes of all trees for providing a combined value that typically varies from zero to one.[44] The increase in complexity enhances the power of discrimination and reduces the chances of overfitting. Nevertheless, as for any machine learning method, it is fundamental to include a cross-validation method to infer or presume external validity of the model. In the current study, the leave-one-out cross-validation (LOOCV) was chosen. The LOOCV method increases computational time and complexity, but also significantly increases the reliability or robustness of the model in classifying new data. Interestingly, TBI accuracy, as presented in Figures 2D and 3, refers to the output values from the LOOCV strategy. This is indeed a slightly pessimistic performance compared to the virtually perfect accuracy that would have been found with the ‘final’ TBI model that is programmed in the commercial Oculus software. Nevertheless, the result from the LOOCV outputs is essentially a more conservative and also a more truthful representation of the generalized performance for the TBI. This is a fundamental consideration that will be addressed in future studies for external validation of TBI, which are already underway.

TBI is a combined parameter based on Scheimpflug-based corneal tomography and biomechanical assessments. It provides exceeding accuracy for detecting ectasia

comparing to other parameters, with high sensitivity for detecting sub-clinical (fruste) ectasia among eyes with normal topography in very asymmetric patients. TBI may also be considered as an objective index for representing the inherent susceptibility of the cornea to undergo ectasia progression, which is highly relevant when screening refractive surgery candidates.

References

1. Binder PS, Lindstrom RL, Stulting RD, et al. Keratoconus and corneal ectasia after LASIK. J Refract Surg 2005;21:749-52.

2. Ambrósio R, Jr., Randleman JB. Screening for ectasia risk: what are we screening for and how should we screen for it? J Refract Surg 2013;29:230-2.

3. Santhiago MR, Smadja D, Wilson SE, Krueger RR, Monteiro ML, Randleman JB. Role of percent tissue altered on ectasia after LASIK in eyes with suspicious topography. J Refract Surg 2015;31:258-65.

4. Santhiago MR, Smadja D, Gomes BF, et al. Association between the percent tissue altered and post-laser in situ keratomileusis ectasia in eyes with normal preoperative topography. Am J Ophthalmol 2014;158:87-95 e1.

5. Ambrósio R, Jr., Dawson DG, Belin MW. Association between the percent tissue altered and post-laser in situ keratomileusis ectasia in eyes with normal preoperative topography. Am J Ophthalmol 2014;158:1358-9.

6. Ambrósio R, Jr., Wilson SE. Complications of laser in situ keratomileusis: etiology, prevention, and treatment. J Refract Surg 2001;17:350-79.

7. McGhee CN, Kim BZ, Wilson PJ. Contemporary Treatment Paradigms in Keratoconus. Cornea 2015;34 Suppl 10:S16-23.

8. Gomes JA, Tan D, Rapuano CJ, et al. Global consensus on keratoconus and ectatic diseases. Cornea 2015;34:359-69.

9. Salomao MQ, Esposito A, Dupps WJ, Jr. Advances in anterior segment imaging and analysis. Curr Opin Ophthalmol 2009;20:324-32.

10. Ambrósio R, Jr., Klyce SD, Wilson SE. Corneal topographic and pachymetric screening of keratorefractive patients. J Refract Surg 2003;19:24-9.

11. Klein SR, Epstein RJ, Randleman JB, Stulting RD. Corneal ectasia after laser in situ keratomileusis in patients without apparent preoperative risk factors. Cornea 2006;25:388-403.

12. Ambrósio R, Jr., Dawson DG, Salomao M, Guerra FP, Caiado AL, Belin MW. Corneal ectasia after LASIK despite low preoperative risk: tomographic and biomechanical findings in the unoperated, stable, fellow eye. J Refract Surg 2010;26:906-11.

13. Chan CC, Hodge C, Sutton G. External analysis of the Randleman Ectasia Risk Factor Score System: a review of 36 cases of post LASIK ectasia. Clin Experiment Ophthalmol 2010;38:335-40.

14. Malecaze F, Coullet J, Calvas P, Fournie P, Arne JL, Brodaty C. Corneal ectasia after photorefractive keratectomy for low myopia. Ophthalmology 2006;113:742-6.

15. Sachdev G, Sachdev MS, Sachdev R, Gupta H. Unilateral corneal ectasia following small-incision lenticule extraction. J Cataract Refract Surg 2015;41:2014-8.

16. Ambrósio R, Jr., Belin MW. Imaging of the cornea: topography vs tomography. J Refract Surg 2010;26:847-9.

17. Saad A, Gatinel D. Topographic and tomographic properties of forme fruste keratoconus corneas. Invest Ophthalmol Vis Sci 2010;51:5546-55.

18. Ambrósio R, Jr., Valbon BF, Faria-Correia F, Ramos I, Luz A. Scheimpflug imaging for laser refractive surgery. Curr Opin Ophthalmol 2013;24:310-20.

19. Smadja D, Touboul D, Cohen A, et al. Detection of subclinical keratoconus using an automated decision tree classification. Am J Ophthalmol 2013;156:237-46 e1.

20. Ambrósio Jr R, Ramos I, Lopes B, et al. Assessing ectasia susceptibility prior to LASIK: the role of age and residual stromal bed (RSB) in conjunction to Belin-Ambrósio deviation index (BAD-D). Revista Brasileira de Oftalmologia 2014;73:75-80.

21. Ambrósio R, Jr., Nogueira LP, Caldas DL, et al. Evaluation of corneal shape and biomechanics before LASIK. Int Ophthalmol Clin 2011;51:11-38.

22. Li Y, Tan O, Brass R, Weiss JL, Huang D. Corneal epithelial thickness mapping by Fourier-domain optical coherence tomography in normal and keratoconic eyes. Ophthalmology 2012;119:2425-33.

23. Reinstein DZ, Gobbe M, Archer TJ, Silverman RH, Coleman DJ. Epithelial, stromal, and total corneal thickness in keratoconus: three-dimensional display with artemis very-high frequency digital ultrasound. J Refract Surg 2010;26:259-71.

24. Pahuja N, Shroff R, Pahanpate P, et al. Application of high resolution OCT to evaluate irregularity of Bowman's layer in asymmetric keratoconus. J Biophotonics 2016.

25. Roberts CJ, Dupps WJ, Jr. Biomechanics of corneal ectasia and biomechanical treatments. J Cataract Refract Surg 2014;40:991-8.

26. Luce DA. Determining in vivo biomechanical properties of the cornea with an ocular response analyzer. J Cataract Refract Surg 2005;31:156-62.

27. Fontes BM, Ambrósio R, Jr., Jardim D, Velarde GC, Nose W. Corneal biomechanical metrics and anterior segment parameters in mild keratoconus. Ophthalmology 2010;117:673-9.

513 28. Luz A, Lopes B, Hallahan KM, et al. Discriminant Value of Custom Ocular
514 Response Analyzer Waveform Derivatives in Forme Fruste Keratoconus. Am J
515 Ophthalmol 2016;164:14-21.
516 29. Luz A, Lopes B, Hallahan KM, et al. Enhanced Combined Tomography and
517 Biomechanics Data for Distinguishing Forme Fruste Keratoconus. J Refract Surg
518 2016;32:479-94.
519 30. Ambrósio Jr R, Ramos I, Luz A, et al. Dynamic ultra high speed Scheimpflug
520 imaging for assessing corneal biomechanical properties. Revista Brasileira de
521 Oftalmologia 2013;72:99-102.
522 31. Ali NQ, Patel DV, McGhee CN. Biomechanical responses of healthy and
523 keratoconic corneas measured using a noncontact scheimpflug-based tonometer.
524 Invest Ophthalmol Vis Sci 2014;55:3651-9.
525 32. Bak-Nielsen S, Pedersen IB, Ivarsen A, Hjortdal J. Dynamic Scheimpflug-based
526 assessment of keratoconus and the effects of corneal cross-linking. J Refract Surg
527 2014;30:408-14.
528 33. Steinberg J, Katz T, Lucke K, Frings A, Druchkiv V, Linke SJ. Screening for
529 Keratoconus With New Dynamic Biomechanical In Vivo Scheimpflug Analyses. Cornea
530 2015;34:1404-12.
531 34. Ambrósio R, Jr., Lopes B, Faria-Correia F, et al. Ectasia Detection by the
532 Assessment of Corneal Biomechanics. Cornea 2016;35:e18-20.
533 35. Vinciguerra R, Elsheikh A, Roberts CJ, et al. Influence of Pachymetry and
534 Intraocular Pressure on Dynamic Corneal Response Parameters in Healthy Patients. J
535 Refract Surg 2016;32:550-61.

536 36. Vicniguerra R, Ambrósio Jr R, Elsheikh A, Roberts CR, Lopes BT, Vinciguerra P.
537 Detection of Keratoconus with the new Corvis ST Biomechanical Index. Journal of
538 Refractive Surgery 2016;in press.
539 37. Lopes BT, Ramos IdC, Salomão MQ, Canedo ALC, Ambrósio Jr. R. Perfil
540 paquimétrico horizontal para a detecção do ceratocone. Revista Brasileira de
541 Oftalmologia 2015;74:382-5.
542 38. Joda AA, Shervin MM, Kook D, Elsheikh A. Development and validation of a
543 correction equation for Corvis tonometry. Comput Methods Biomech Biomed Engin
544 2016;19:943-53.
545 39. Lopes B, Ramos ICdO, Ribeiro G, et al. Bioestatísticas: conceitos fundamentais
546 e aplicações práticas. Revista Brasileira de Oftalmologia 2014;73:16-22.
547 40. Gomes JA, Tan D, Rapuano CJ, et al. Global consensus on keratoconus and
548 ectatic diseases. Cornea 2015;34:359-69.
549 41. Rabinowitz YS. Keratoconus. Surv Ophthalmol 1998;42:297-319.
550 42. Rabinowitz YS, Rasheed K. KISA% index: a quantitative videokeratography
551 algorithm embodying minimal topographic criteria for diagnosing keratoconus. J
552 Cataract Refract Surg 1999;25:1327-35.
553 43. Ramos IC, Correa R, Guerra FP, et al. Variability of subjective classifications of
554 corneal topography maps from LASIK candidates. J Refract Surg 2013;29:770-5.
555 44. Breiman L. Random Forests. Machine Learning 2001;45:5-32.
556 45. Ambrósio R, Jr., Luz A, Lopes B, Ramos I, Belin MW. Enhanced ectasia
557 screening: the need for advanced and objective data. J Refract Surg 2014;30:151-2.

558 46. Ambrósio R, Jr., Ramos I, Lopes B, et al. Ectasia susceptibility before laser
559 vision correction. J Cataract Refract Surg 2015;41:1335-6.
560 47. Belin MW, Ambrósio R. Scheimpflug imaging for keratoconus and ectatic
561 disease. Indian J Ophthalmol 2013;61:401-6.
562 48. Belin MW, Villavicencio OF, Ambrósio RR, Jr. Tomographic parameters for the
563 detection of keratoconus: suggestions for screening and treatment parameters. Eye
564 Contact Lens 2014;40:326-30.
565 49. DeLong ER, DeLong DM, Clarke-Pearson DL. Comparing the areas under two or
566 more correlated receiver operating characteristic curves: a nonparametric approach.
567 Biometrics 1988;44:837-45.
568 50. Buhren J, Kuhne C, Kohnen T. Defining subclinical keratoconus using corneal
569 first-surface higher-order aberrations. Am J Ophthalmol 2007;143:381-9.
570 51. Salomao MQ, Ramos IC, Jordao LF, Canedo ALC, Valbon BF, Luz A, Correa R,
571 Lopes BT, Ambrósio Jr R. Accuracy of Topometric Indices for Distinguishing between
572 Keratoconic and Normal Corneas. Int J Keratoconus and Ectatic Corneal Diseases
573 2013;2:108-12.
574 52. Arbelaez MC, Versaci F, Vestri G, Barboni P, Savini G. Use of a support vector
575 machine for keratoconus and subclinical keratoconus detection by topographic and
576 tomographic data. Ophthalmology 2012;119:2231-8.
577 53. Klyce SD. Chasing the suspect: keratoconus. Br J Ophthalmol 2009;93:845-7.
578 54. Ramos IC, Reinstein DZ, Archer T, Gobbe M, Salomão MQ, Lopes BT, Luz A,
579 Faria-Correia F, Gatinel D, Belin MW, Ambrósio Jr R. Unilateral Ectasia characterized

by Advanced Diagnostic Tests. International Journal of Keratoconus and Ectatic Corneal Diseases 2016;5:51-56.

Figure legends

Figure 1: Front surface axial or sagittal curvature (topometric) maps using Smolek-Klyce absolute 1.5D scale from the 94 cases included in Group IV (VAE-NT).

Figure 2: box and dot plots showing the distribution of metric values across the groups. **A,** BADD **B,** BADDI **C,** CBI **D,** LRI **E,** SVMI **F,** TBI. The box spans the 1st and 3rd quartile. the whiskers indicate the 1.5-fold interquartile range. Colored markers representing each value and their mean are superimposed.

Figure 3: receiver-operating characteristic and separation curves for the different metrics. **A,** group I (normals) vs. groups II (keratoconus), III (very asymmetric ectasia) and IV (topographically normal fellow eyes of very asymmetric ectasia eyes) **B,** group I vs. groups II and III **C,** group I vs. groups IV.

Tables

Table 1. Demographic Characteristics of the Groups

	RIO				Milano			
	n	Male	Female	Ave Age (min - max)	n	Male	Female	Ave Age (min - max)
group I (normals)	227	96	131	37.71 (7 – 90)	253	108	145	43.20 (7 – 88)
group II (KC eyes)	111	72	39	32.90 (12 – 64)	93	66	27	38.10 (16 – 72)
group III (E-VAE eyes)	19	10	9	32.89 (14 – 74)	53	30	23	36.96 (13 – 83)
group IV (NT-VAE eyes)	26	15	11	35.02 (14 – 74)	68	39	29	37.66 (13 – 83)

Table 2: Descriptive statistics. Mean ± standard deviation; median (minimum – maximum)

	group I (normals)	***group II (KC eyes)***	***group III (E-VAE eyes)***	***group IV (NT-VAE)***
I-S Value	0.16 ±0.55	5.79 ±4.32	5.17 ±3.63	0.53 ±0.51
	0.16 (-1.46 - 1.91)	4.80 (-2.60 - 33.69)	4.34 (-2.07 - 16.07)	0.61 (-0.76 - 1.42)
KISA	10.73 ±13.95	2699.29 ±12870.32	1579.36 ±4666.63	13.81 ±14.88
	5.24 (0.33 - 82.62)	369.72 (2.30 - 173021)	285.03 (2.79 - 35153)	7.51 (0.33 - 59.20)
Pachy Min	552.56 ±29.99	466.86 ±47.84	480.11 ±42.14	517.66 ±30.95
	553 (467 - 646)	468.50 (173 - 596)	479.50 (351 - 581)	521 (449 - 599)
Pachy Apex	558.45 ±30.10	488.60 ±123.24	493.85 ±43.37	525.98 ±29.68
	559 (470 - 647)	485 (209 - 213)	492.50 (356 - 583)	529 (451 - 606)
ART Max	469.84 ±76.56	177.63 ±76.08	197.58 ±88.84	369.89 ±77.23
	463 (247 - 744)	166.50 (0.00 - 460)	174 (66.00 - 442)	365 (190 - 546)
ART Avg	601.90 ±93.58	261.34 ±104.37	292.61 ±110.97	491.43 ±78.47
	591.50 (359 - 985)	259.50 (0.00 - 653)	270.50 (101 - 609)	487.5 (298 - 667)
EleF BFS8mm Thinnest	1.90 ±1.63	19.60 ±19.33	19.00 ±10.46	2.83 ±1.74
	2.00 (-4.00 - 8.00)	16.50 (-50.00 - 72.00)	16.50 (0.00 - 49.00)	3.00 (-2.00 - 9.00)
EleB BFS 8mmThinnest	6.04 ±4.40	56.04 ±125.78	44.47 ±20.86	9.39 ±5.21
	6.00 (-5.00 - 19.00)	42.00 (2.00 - 1805.00)	43.00 (12.00 - 95.00)	9.00 (1.00 - 27.00)
SP_A1	106.30 ±17.65	66.84 ±24.11	67.25 ±24.90	85.19 ±26.04
	104.81 (60.69 - 165.00)	66.72 (2.91 - 150.11)	65.66 (32.33 - 116.74)	89.29 (35.22 - 142.45)
DARatioMax 2mm	4.30 ±0.50	5.86 ±1.56	5.53 ±1.21	4.83 ±0.64
	4.30 (3.19 – 5.60)	5.58 (3.20 – 15.36)	5.33 (3.55 – 8.77)	4.71 (3.68 – 6.52)
MaxInverse Radius Gauss5Fmm1	0.16 ±0.02	0.21 ±0.05	0.20 ±0.04	0.17 ±0.02
	0.15 (0.08 – 0.24)	0.20 (0.12 – 0.51)	0.19 (0.12 – 0.31)	0.17 (0.12 – 0.28)
BAD-D	0.75 ±0.56	7.97 ±4.66	6.97 ±3.64	1.61 ±0.68
	0.8 (1.13 - 2.35)	6.93 (0.76 - 25.94)	6.37 (1.82 - 18.79)	1.53 (0.18 - 3.22)
BAD-DI	0.12 ±0.14	0.98 ±0.11	0.99 ±0.06	0.44 ±0.31
	0 (0.070 - 0.87)	1 (0.06 – 1)	1 (0.59 – 1)	0.38 (0.01 - 0.99)
CBI	0.06 ±0.14	0.92 ±0.22	0.91 ±0.24	0.41 ±0.4
	0 (0 - 0.88)	1 (0 – 1)	1 (0 – 1)	0.24 (0 – 1)
LRAI	0.11 ±0.15	0.88 ±0.26	0.81 ±0.33	0.87 ±0.28
	0 (0.050 - 0.79)	1 (0.03 – 1)	1 (0.02 – 1)	1 (0.02 – 1)
SVMI	0.1 ±0.11	0.88 ±0.28	0.81 ±0.35	0.88 ±0.3
	0.08 (0.04 - 0.95)	1 (0.07 – 1)	1 (0.05 – 1)	1 (0.04 – 1)
TBI	0.07 ±0.1	0.97 ±0.04	0.97 ±0.04	0.76 ±0.28
	0 (0.070 - 0.75)	0.97 (0.83 – 1)	0.97 (0.87 – 1)	0.76 (0.08 – 1)

KC: keratoconus, VAE-E: ectatic eye from patients with very asymmetric ectasia, VAE-NT: normal topography fellow eye from patients with very asymmetric ectasia. BAD-D: Belin/Ambrósio Deviation value; BAD-DI: Belin/Ambrósio Deviation normalized index; CBI: Corvis Biomechanical Index; DA Ratio 2mm: deformation amplitude ratio between the apex and at 2mm from the apex; I-S: paracentral inferior–superior asymmetry value at 6mm (3mm radii); KISA: keratoconus percentage index; LRAI: linear regression analysis index; MaxInverse Radius: inverse of maximal inverse radius at highest concavity; Pachy Apex: pachymetric

value at the corneal apex: Pachy Min: pachymetric value at the corneal apex; SPA1: stiffness parameter at first applanation; SVMI: support vector machine; TBI: tomographic & biomechanical index.

Table 3: Results of receiver-operating characteristic (ROC) curve analysis.

A. groups I vs. [II,III,IV]: normal vs. 'diseased' (KC, E-VAE and NT-VAE fellow eyes; Figure 2A)

Parameter	*AUROC*	*Sensitivity*	*Specificity*	*correctly classified [%]*	*cutoff*	*specificity @ 100% sensitivity*	*AUSEP*
BAD-D	0.956	0.841	0.965	90.3	1.62	14	51
BAD-DI	0.956	0.841	0.965	90.3	0.45	14	83
CBI	0.937	0.808	0.971	88.9	0.46	0	82
LRAI	0.967	0.884	0.960	92.2	0.44	31	95
SVMI	0.964	0.868	0.975	92.1	0.34	1	105
TBI	0.996	0.962	0.988	97.5	0.48	72	110

B. groups I vs. [II,III]: normal vs. frank ectasia (KC and E-VAE eyes; Figure 2B)

parameter	*AUROC*	*sensitivity*	*specificity*	*correctly classified [%]*	*cutoff*	*specificity @ 100% sensitivity*	*AUSEP*
BAD-D	0.997	0.982	0.992	98.7	1.97	47.3	64
BAD-DI	0.997	0.982	0.992	98.7	0.69	47.3	95
CBI	0.977	0.946	0.975	96.0	0.49	12.9	95
LRAI	0.967	0.888	0.960	92.4	0.44	32	99
SVMI	0.964	0.877	0.967	92.2	0.30	1	109
TBI	1.000	1.000	1.000	100.0	0.79	100	112

C. groups I vs. IV: normal vs. NT- VAE fellow eyes (Figure 2C)

parameter	*AUROC*	*sensitivity*	*specificity*	*correctly classified [%]*	*cutoff*	*specificity @ 100% sensitivity*	*AUSEP*
BAD-D	0.838	0.809	0.717	76.3	1.08	14	49
BAD-DI	0.838	0.809	0.717	76.3	0.14	14	47
CBI	0.822	0.681	0.823	75.2	0.07	0	46
LRAI	0.968	0.872	0.969	92.1	0.51	31	125
SVMI	0.965	0.851	1.000	92.6	0.96	1	79
TBI	0.985	0.904	0.960	93.2	0.29	71.9	99

KC: keratoconus, E-VAE: ectatic eye from patients with very asymmetric ectasia, NT-VAE: normal topography fellow eye from patients with very asymmetric ectasia, AUROC area under the ROC curve, AUSEP: area under the separation curve

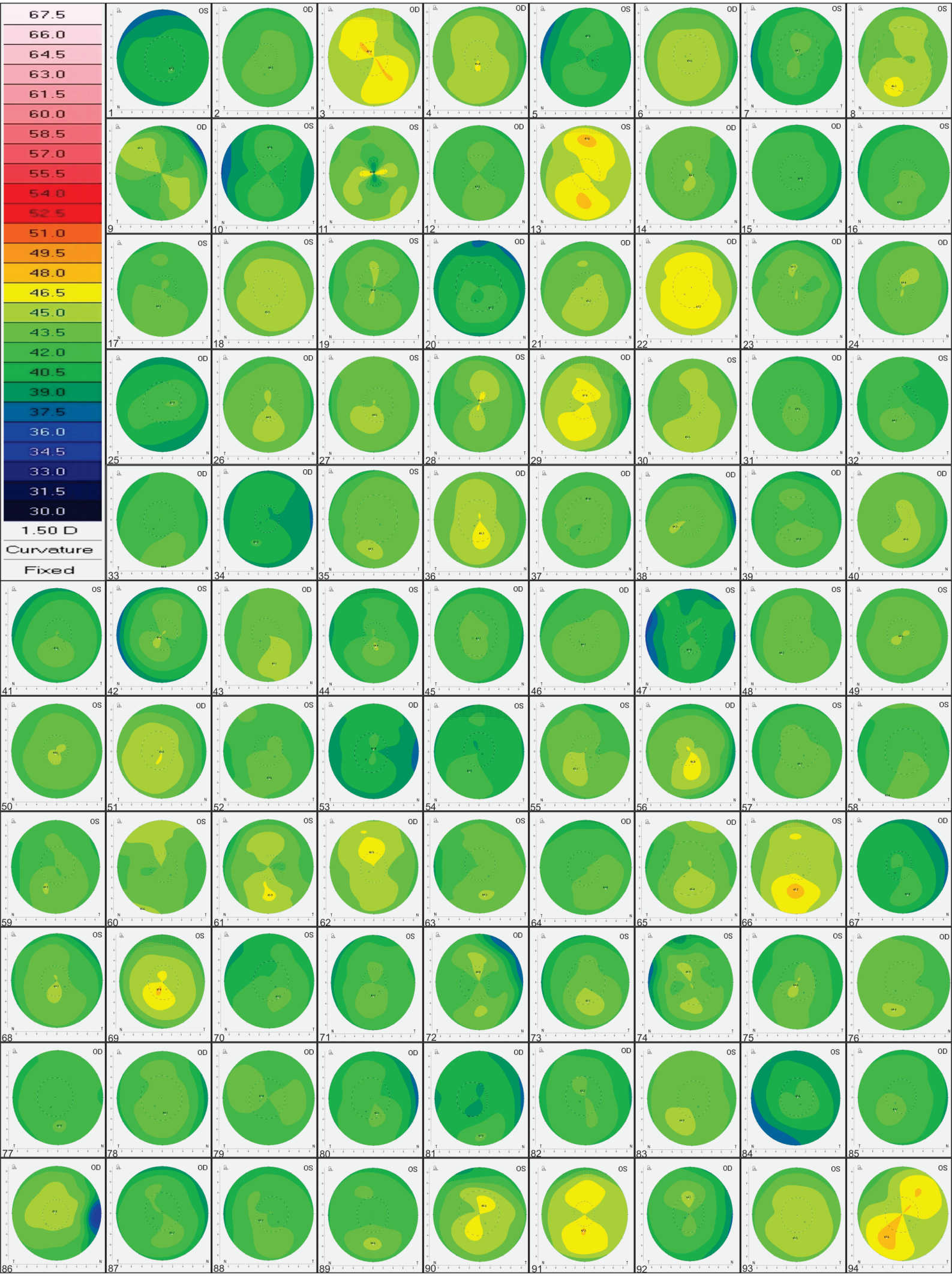
67.5
66.0
64.5
63.0
61.5
60.0
58.5
57.0
55.5
54.0
52.5
51.0
49.5
48.0
46.5
45.0
43.5
42.0
40.5
39.0
37.5
36.0
34.5
33.0
31.5
30.0
1.50 D
Curvature
Fixed

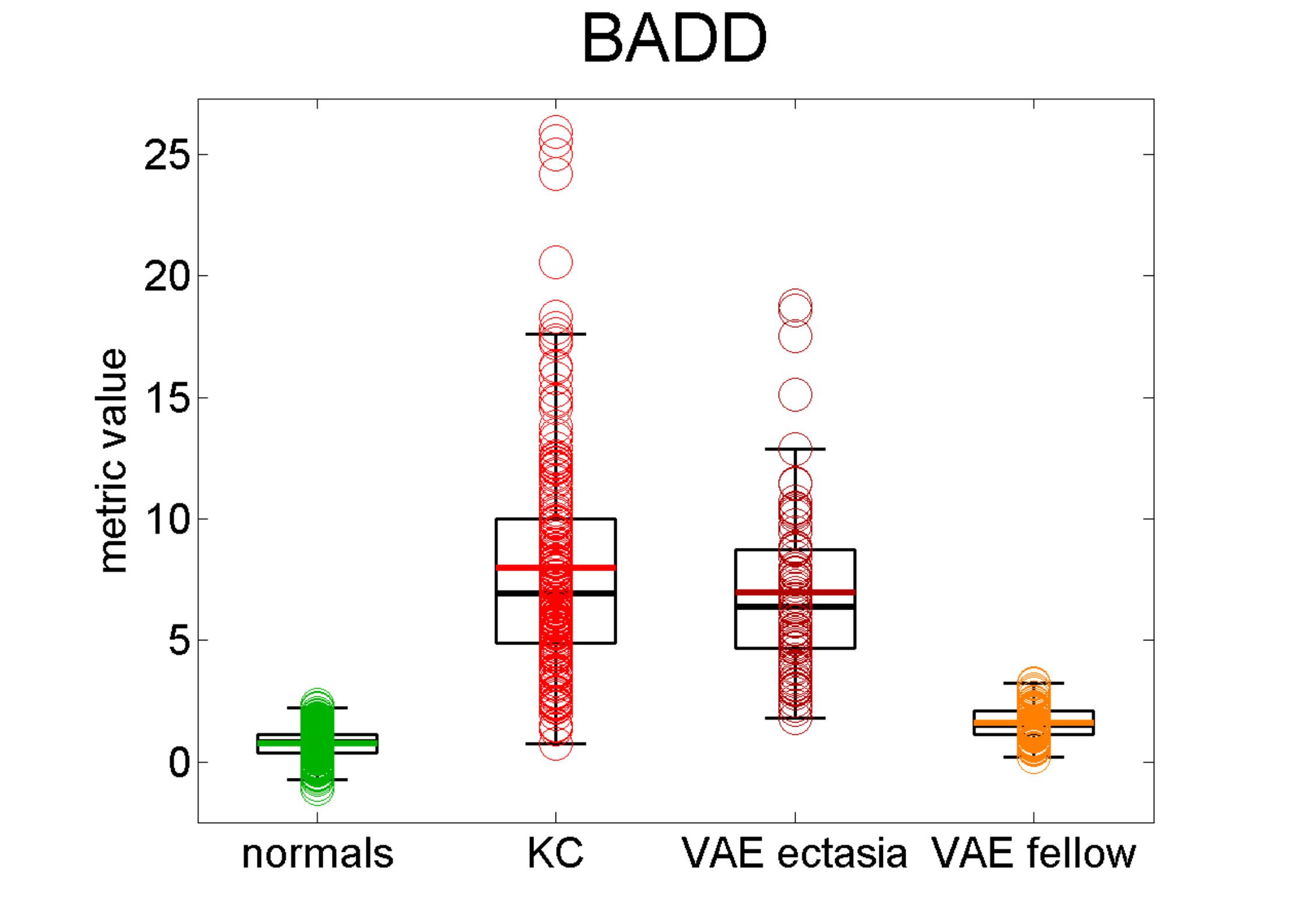
BADD
metric value
25
20
15
10
5
0
normals
KC
VAE ectasia
VAE fellow

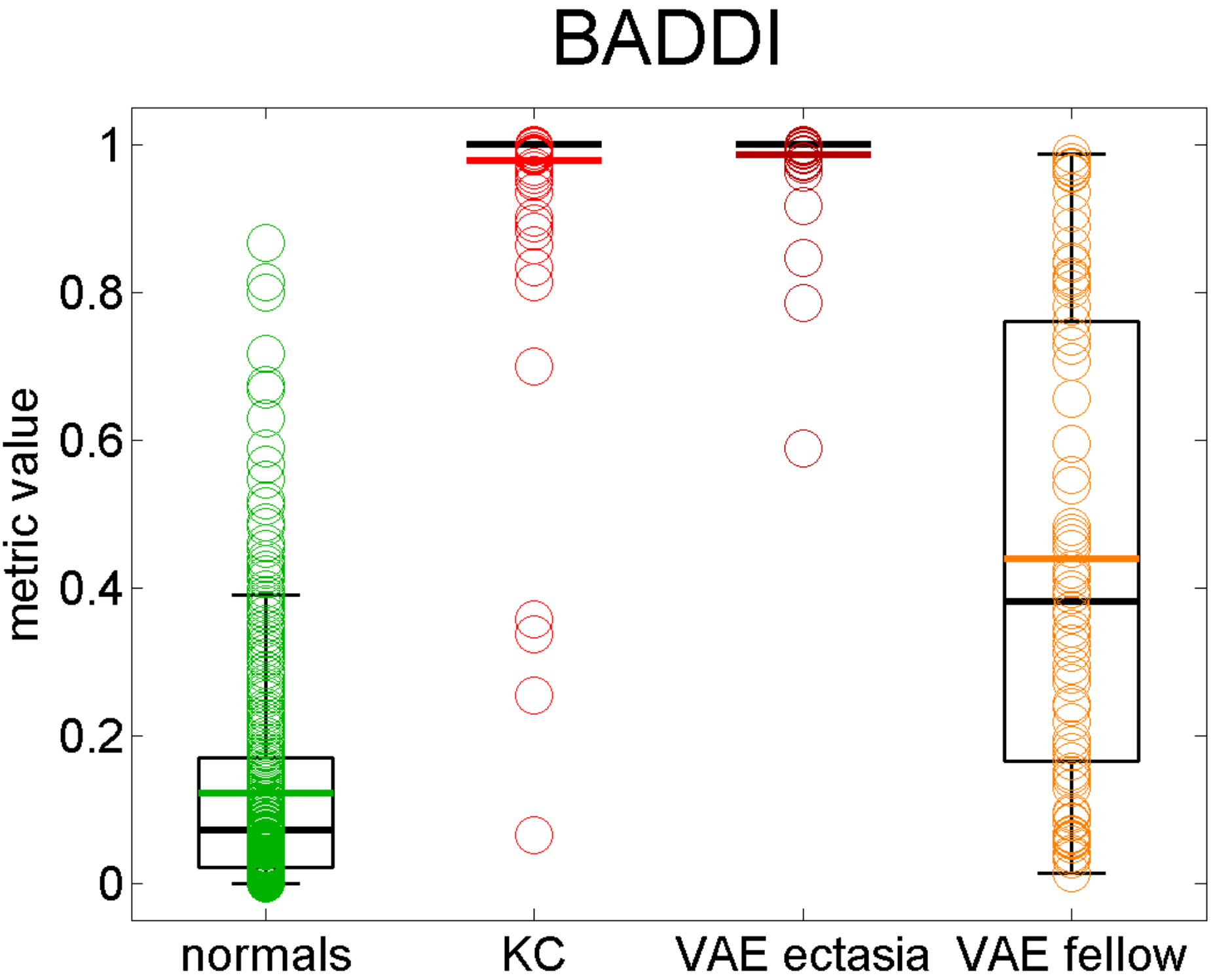
BADDI
metric value
1
0.8
0.6
0.4
0.2
0
normals
KC
VAE ectasia
VAE fellow

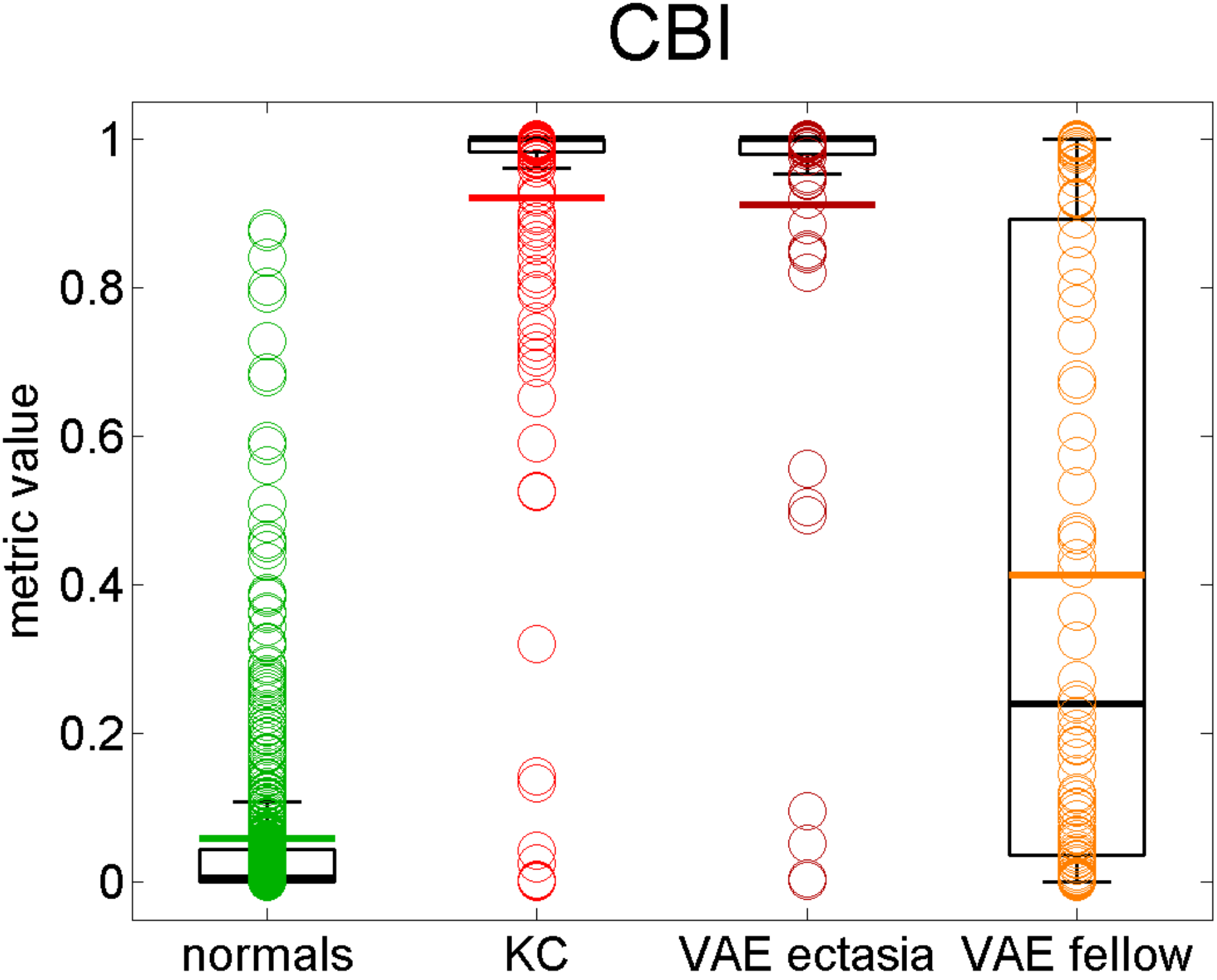
CBI
metric value
1
0.8
0.6
0.4
0.2
0
normals
KC
VAE ectasia
VAE fellow

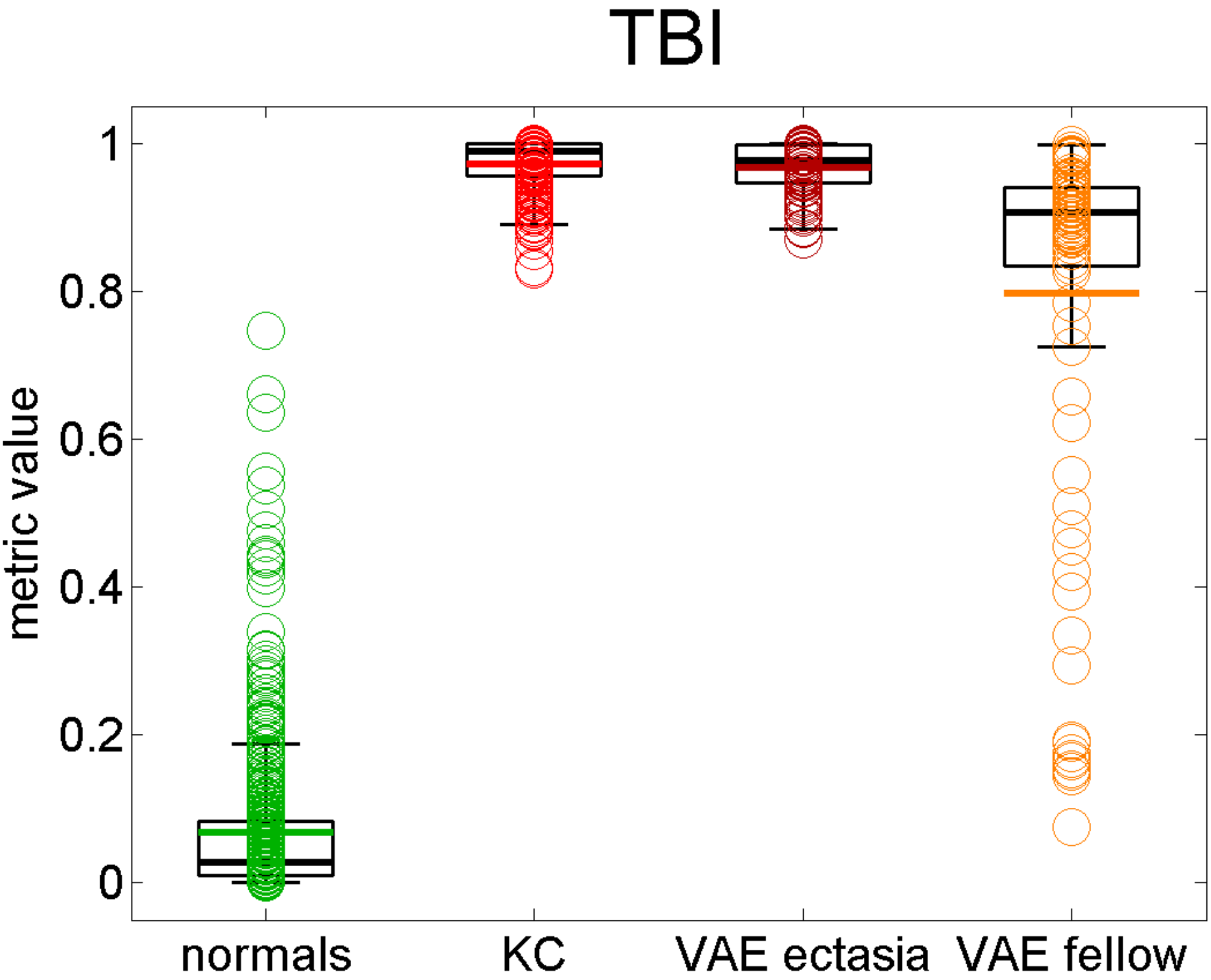
TBI
metric value
1
0.8
0.6
0.4
0.2
0
normals
KC
VAE ectasia
VAE fellow

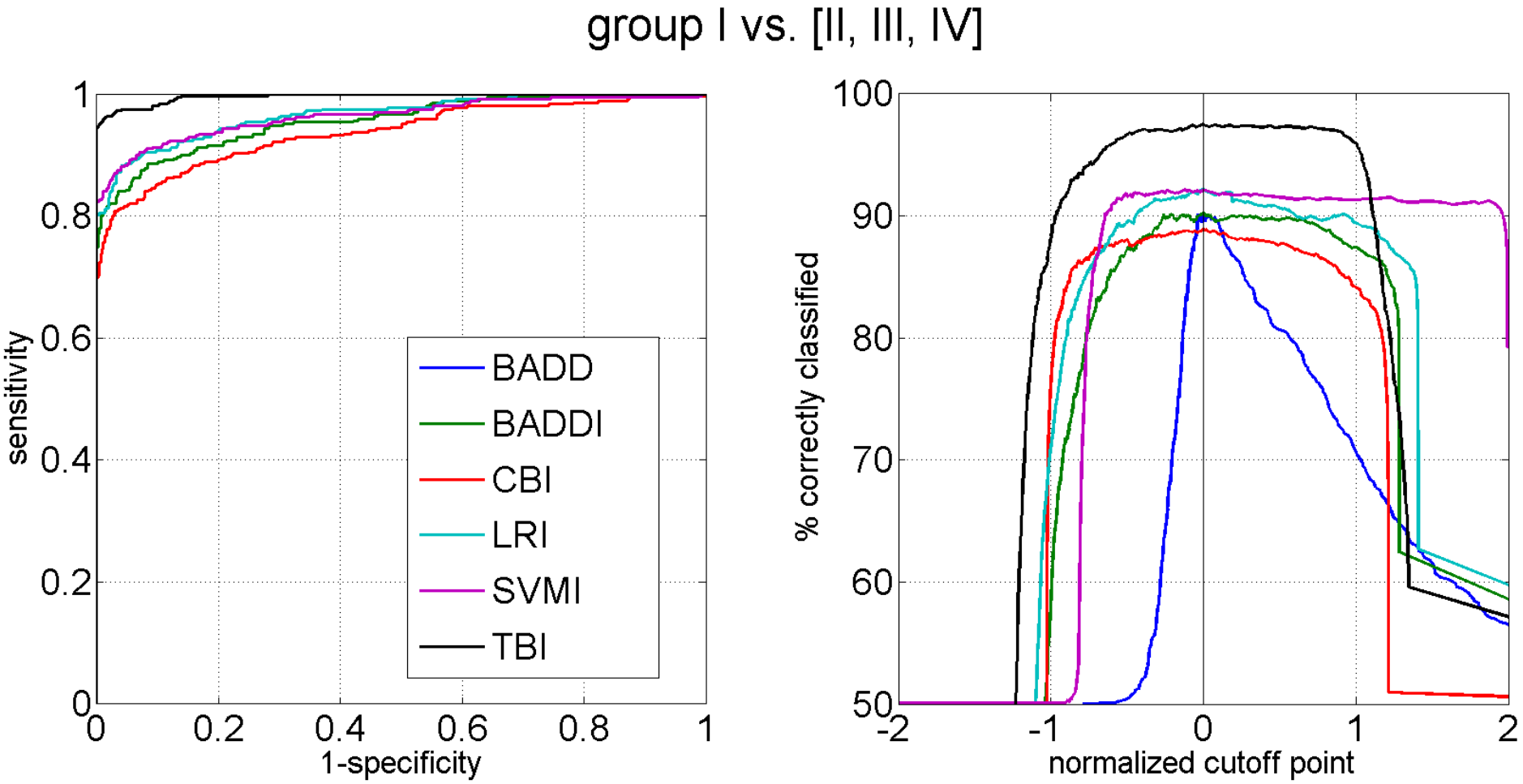
group I vs. [II, III, IV]
sensitivity
1-specificity
0
0.2
0.4
0.6
0.8
1
BADD
BADDI
CBI
LRI
SVMI
TBI
% correctly classified
normalized cutoff point
50
60
70
80
90
100
-2
-1
0
1
2

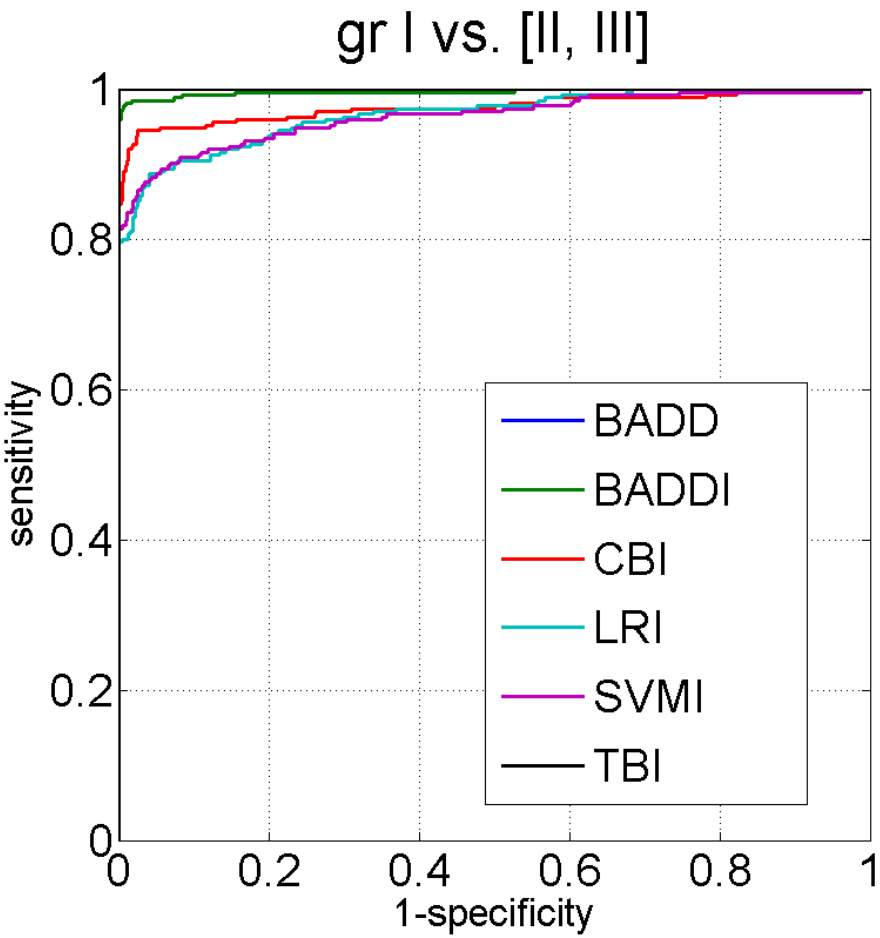
gr I vs. [II, III]
sensitivity
1-specificity
0
0.2
0.4
0.6
0.8
1
BADD
BADDI
CBI
LRI
SVMI
TBI

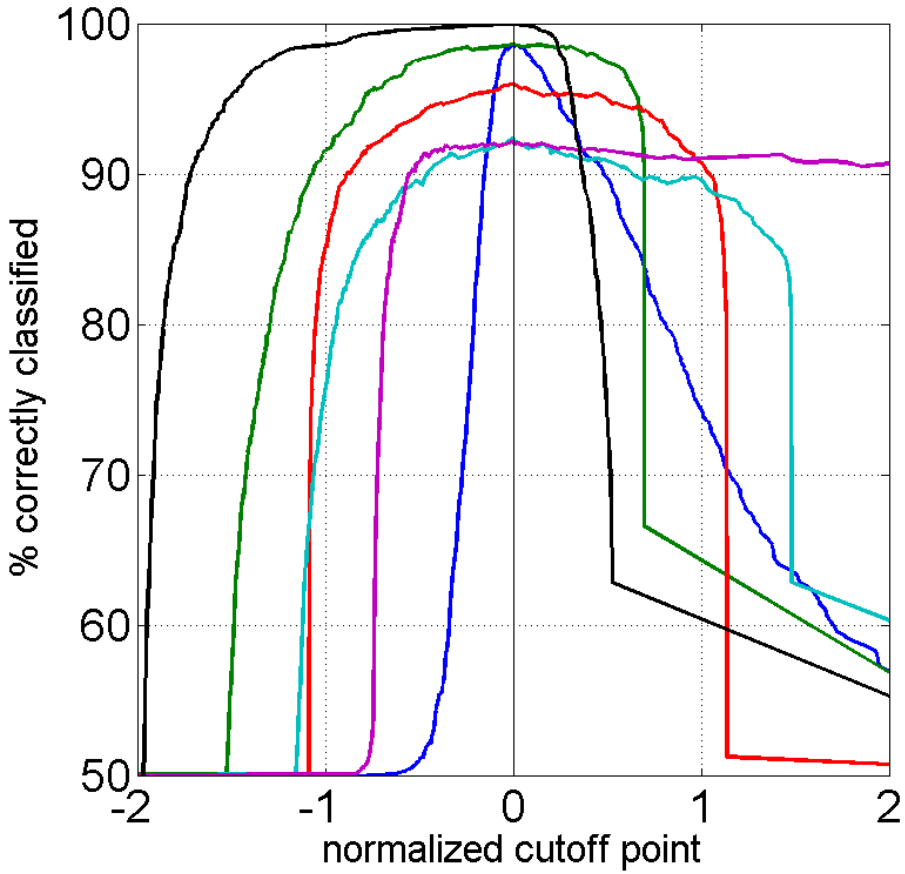
% correctly classified
normalized cutoff point
100
90
80
70
60
50
-2
-1
0
1
2

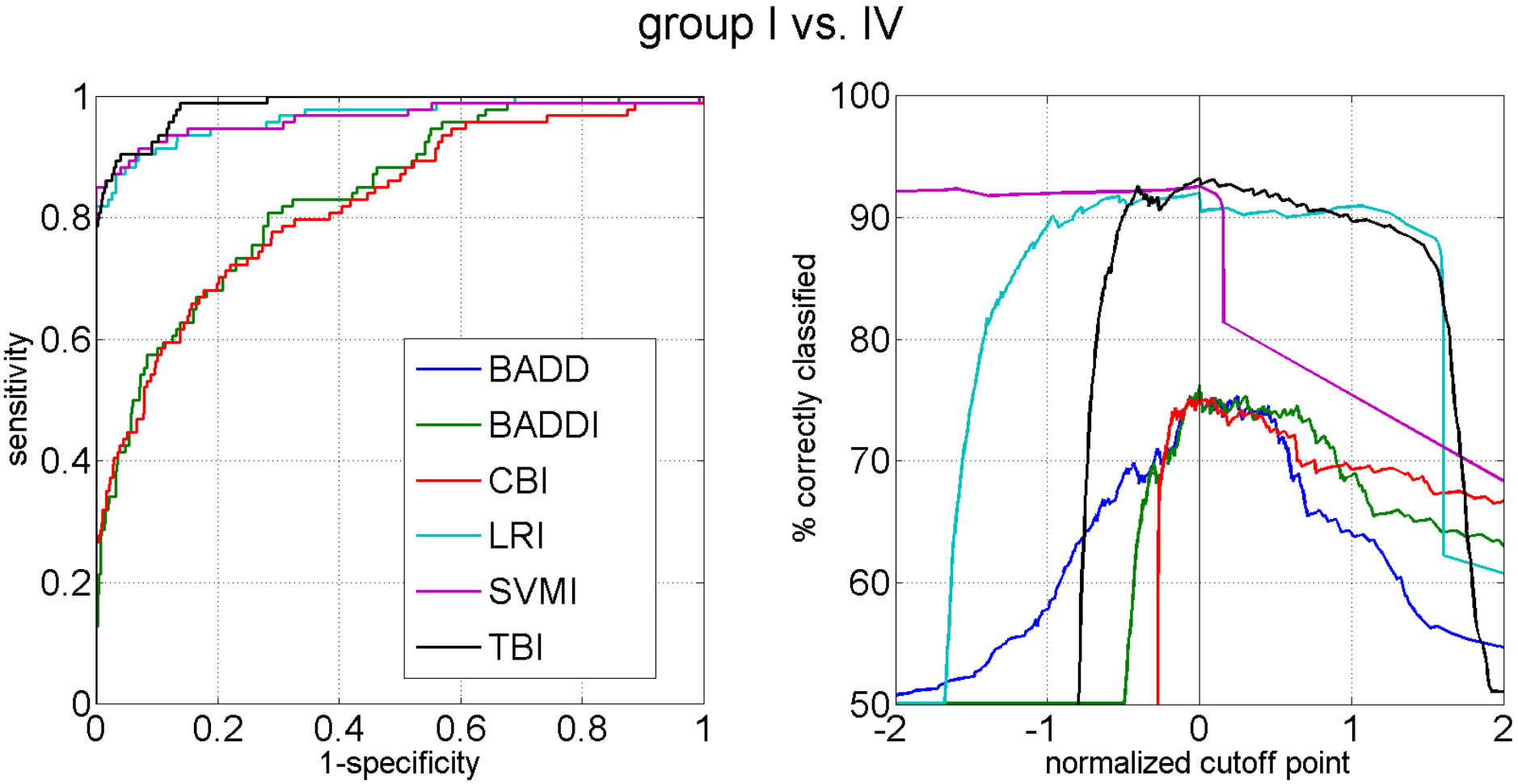
group I vs. IV
sensitivity
1-specificity
0
0.2
0.4
0.6
0.8
1
BADD
BADDI
CBI
LRI
SVMI
TBI
% correctly classified
normalized cutoff point
100
90
80
70
60
50
-2
-1
0
1
2